HHS Public Access

Author manuscript

Biochim Biophys Acta. Author manuscript; available in PMC 2018 November 01.

Published in final edited form as:

Biochim Biophys Acta. 2017 November ; 1863(11): 2862–2870. doi:10.1016/j.bbadis.2017.07.020.

Genetic Ataxia Telangiectasia porcine model phenocopies the multisystemic features of the human disease

Rosanna Beraldi[a], **David K. Meyerholz**[b], **Alexei Savinov**[a], **Attila D. Kovács**[a,c], **Jill M. Weimer**[a,c], **Jordan A. Dykstra**[a], **Ryan D. Geraets**[a,c], and **David A. Pearce**[a,c]

[a]Pediatric and Rare Diseases Group, Sanford Research, Sioux Falls, SD 57104, USA

[b]Department of Pathology, University of Iowa, Iowa City, IA 52242, USA

[c]Sanford School of Medicine at the University of South Dakota, Sioux Falls, SD 57105, USA

Abstract

Ataxia telangiectasia (AT) is a progressive multisystem autosomal recessive disorder caused by mutations in the *AT-mutated* (*ATM*) gene. Early onset AT in children is characterized by cerebellar degeneration, leading to motor impairment. Lung disease and cancer are the two most common causes of death in AT patients. Accelerated thymic involution may contribute to the cancer, and recurrent and/or chronic respiratory infections may be a contributing factor to lung disease in AT. AT patients have fertility issues, are highly sensitive to ionizing radiation and they present oculocutaneous telangiectasia. Current treatments only slightly ameliorate disease symptoms; therapy that alters or reverses the course of the disease has not yet been discovered. Previously, we have shown that $ATM^{-/-}$ pigs, a novel model of AT, present with a loss of Purkinje cells, altered cerebellar cytoarchitecture and motor coordination deficits. $ATM^{-/-}$ porcine model not only recapitulates the neurological phenotype, but also other multifaceted clinical features of the human disease. Our current study shows that $ATM^{-/-}$ female pigs are infertile, with anatomical and functional signs of an immature reproductive system. Both male and female $ATM^{-/-}$ pigs show abnormal thymus structure with decreased cell cycle and apoptosis markers in the gland. Moreover, $ATM^{-/-}$ pigs have an altered immune system with decreased $CD8^+$ and increased natural killer and $CD4^+CD8^+$ double-positive cells. Nevertheless, $ATM^{-/-}$ pigs manifest a deficient IgG response after a viral infection. Based on the neurological and peripheral phenotypes, the $ATM^{-/-}$ pig is a novel genetic model that may be used for therapeutic assessments and to identify pathomechanisms of this disease.

Keywords

neurodegenerative; infertility; immunology; thymus; p53

[*]**Address correspondence to:** David A. Pearce, Sanford Research, 2301 E. 60 Street North, Sioux Falls, SD 57104, USA, David.Pearce@SanfordHealth.org, Phone: 1-(605)312-6004.

CONFLICT OF INTEREST

None

INTRODUCTION

Ataxia telangiectasia (AT) is a genetic multisystem disorder affecting one in 40,000–100,000 live births (1). The disease begins during childhood with motor coordination impairment resulting predominantly from Purkinje cell loss in the cerebellum, and progresses as a multisystemic disease (2, 3). AT patients show: sensitivity to radiation, fertility problems, thymic atrophy/hypoplasia, tumor development (mainly of lymphoid organs) (4, 5), recurrent respiratory infections and immunologic deficiencies (6). Immunodeficiency is likely result of the abnormal thymic development and function. Autopsy reports of patients commonly show absence or hypoplasia of the gonads corresponding to sterility (7). Lung disease and cancer are the two most common causes of death (8, 9). Current treatments only slightly ameliorate disease symptomatology, and no cure to alter or reverse the course of the disease has been discovered.

Mutations in the *ATM* gene are associated with the clinical manifestations of AT disease and 80% of AT patients have a non-functional ATM protein. ATM is a ubiquitous protein that functions as a DNA damage response sentinel in several organ systems and at many different cell stages from mitotically inactive to dividing cells (10–13). However, how lack of ATM can produce a progressive, pleiotropic disease and the underlying mechanisms are still unknown.

Several small animal models (mouse, rat, zebrafish and Drosophila) successfully recapitulating primary and secondary features of AT have been established over the last 2 decades (14–17). However, a large animal model more similar to humans in terms of size, age, and physiology would model the disease better, helping to facilitate basic and translational research in the AT field. For this purpose, we have genetically engineered the first porcine model of AT by eliminating the kinase domain from the porcine *ATM* gene. We have previously demonstrated that this model recapitulates the cerebellar defects seen in human disease i.e. loss of Purkinje cells and motor deficits (18). However, due to the pleiotropic character of AT, the $ATM^{-/-}$ porcine model must demonstrate other clinical manifestations to be considered a valuable model of the human disease. In the current manuscript, we show that our porcine model of AT recapitulates not only the cerebellar deficits, but also several other pathological features of human AT, including sterility, accelerated thymic involution, and immunological defects. Together, these new findings corroborate our model as the first genetic large animal model of AT and expand the future of translational research for this disease.

RESULTS

Structural and functional abnormalities in the reproductive system of $ATM^{-/-}$ female pigs

Necropsies of wild-type (WT) and $ATM^{-/-}$ female pigs (n=3 WT and 3 $ATM^{-/-}$ pigs at 1 month and 1 year; n=1 WT and 1 *ATM*−/− pigs at 2.5 years) were performed for all organs. All the organs were comparable between the two pig groups in terms of macroscopic and microscopic anatomy. However, one-year-old $ATM^{-/-}$ females had smaller ovaries and uteri (Fig. 1A and Supplementary Fig. 1), recapitulating what has been shown in AT patients (19–

21); no gross abnormalities were found at 1 month of age. Histochemical staining including the gold standard hematoxylin and eosin (H&E) was performed for routine microscopic tissue examination. H&E staining of ovaries from one-month-old WT and *ATM*$^{-/-}$ females did not show statistically significant differences in terms of size and structure (Supplementary Fig. 2). Ovaries from one-month-old animals of both groups were composed primarily of fibrovascular tissue stroma with primordial follicles especially noted in the cortex (Fig. 1B). By one year of age, WT ovaries had various stages of follicular development as expected for a sexually-mature and cycling female (Fig. 1C, upper left and middle images). Conversely, *ATM*$^{-/-}$ ovaries were small and composed of cortical cords/nests (Fig 1C arrows) on a fibrovascular stroma (Fig 1C asterisks). *ATM*$^{-/-}$ ovaries lacked the expected stages of follicular development for a sexually mature female and instead had large cells adjacent to the cortical cords, which were reminiscent of primordial follicle cells (arrows in the bottom right image of Fig. 1C). Some of these cells were morphologically degenerate compared to WT primordial follicles (Fig. 1C, right images) consistent with cell death (Fig. 1C, bottom right image: inset, arrowhead). At the same age (1 year), the *ATM*$^{-/-}$ uterus was hypoplastic but presented typical structure of the WT in preserving the major components: perimetrium, myometrium and endometrium (Supplementary Fig. 1). To assess whether the abnormalities in the *ATM*$^{-/-}$ ovary and uterus were associated with hormone production issues, the level of circulating estradiol (E2) was measured in sexually mature WT and *ATM*$^{-/-}$ female pigs. Furthermore, the pigs were monitored for clinical signs of estrus, defined as red and swollen vulva, clear discharge, and interest in mating with males. *ATM*$^{-/-}$ females had undetectable amounts of estradiol in the blood (Fig. 1D), lacked clinical signs of an active estrous cycle and were never able to produce progeny after mating with healthy, control males.

To determine if *ATM*$^{-/-}$ males manifested similar fertility problems, semen was collected from three WT and two *ATM*$^{-/-}$ males. The number of males in the current study was limited because male pigs are often castrated at birth, which is a routine management procedure. Assessment of the semen revealed no difference in the motility and number of spermatozoa between the two groups. However, *ATM*$^{-/-}$ males, presented spermatozoa with cytoplasmic droplets (Supplemental Fig. 3A). The boars were also assayed for their ability to impregnate female and produce offspring (Supplementary Fig. 3B). There was a trend toward lower conception rate as well as smaller litter size when *ATM*$^{-/-}$ males were used versus WT males.

Thymic abnormalities in *ATM*$^{-/-}$ pigs

The thymus has been shown to be absent or smaller and microscopically abnormal in autopsies of AT patients (22, 23). To determine whether the *ATM*$^{-/-}$ porcine model recapitulates the same human features, we necropsied *ATM*$^{-/-}$ and WT pigs at one month and one year of age. Examination of all *ATM*$^{-/-}$ thymi at 1 month and 1 year did not show significant macroscopic differences compared to the thymi from gender- and age-matched WT pigs. The thymi were processed and stained (H&E) for histopathology and morphometric analysis. The *ATM*$^{-/-}$ thymus at 1 year of age appeared to have more infiltration of adipose tissue in lobules as often seen during thymic involution; however, the morphometric analysis showed that the difference was not statistically significant (Fig. 2A,

images and lower right graph). At one year of age, the cortex was similar in extent between groups, but *ATM*$^{-/-}$ pigs had reduced medulla area as well as medulla:cortex ratio in the thymus ($p<0.05$, unpaired t-test) (Fig. 2A, upper graphs). Interestingly, the number of the Hassel's corpuscles was also reduced in the medulla of the *ATM*$^{-/-}$ thymus ($p<0.05$) (Fig. 2A, lower left and middle graphs). Morphometric analysis of the thymus at one month of age did not show differences between *ATM*$^{-/-}$ and WTs (data not shown). Fig 2B shows the thymus of an *ATM*$^{-/-}$ pig that was euthanized at 2.5 years of age after natural infection with -porcine reproductive and respiratory syndrome virus (PRRS). Necropsy revealed that the thymus of this *ATM*$^{-/-}$ pig was smaller with more adipose tissue compared to an age-matched thymus WT pig also infected with PRRS (Fig. 2B). H&E staining of the *ATM*$^{-/-}$ thymus tissue similarly showed abundant adipose tissue, small aggregates of lymphoid tissue (with rare evidence of thymic cortex and medulla) and some scattered pigmented melanocytes (Fig. 2B). No morphometric measurements were possible due to the lack of the normal architecture. Altogether, the abnormal and progressive features found in the thymus of *ATM*$^{-/-}$ pigs parallels what has been found in AT patients (22, 23).

Decreased apoptosis and cell cycle arrest in *ATM*$^{-/-}$ thymus

To better elucidate the pathology of the thymus in *ATM*$^{-/-}$ pigs, we performed Western blotting using antibodies against apoptotic proteins (total and cleaved caspase 3) and cell cycle proteins [Cdk2, p21, total p53, phospho-p53(Ser15) and phospho-p53(Ser20)]. We observed reduced cleaved caspase 3 levels with expected accumulation of the uncleaved form in the *ATM*$^{-/-}$ samples (Fig. 3A). Cleaved caspase 3 was undetectable or very low expressed in the spleen and pancreas (Supplementary Fig. 4B), which were used as control organs. Cdk2 and p21 expression was also decreased in the *ATM*$^{-/-}$ thymus (Fig. 3A). In contrast, there was an increase in the level of total p53 in all *ATM*$^{-/-}$ thymi. Interestingly, Western blotting for p53 showed two bands, one at the correct molecular weight and one band slightly higher, suggesting the presence of phosphorylated forms of p53. The higher molecular-weight band was reduced in *ATM*$^{-/-}$ samples (Fig. 3A). Because Ser15 and Ser20 of p53 are ATM targets (18), we tested their phosphorylation by Western blotting. However, phospho-p53(Ser15) and phospho-p53(Ser20) were undetectable in both WT and *ATM*$^{-/-}$ thymic lysates (Supplementary Fig. 4A).

We next performed immunohistochemistry for cleaved caspase 3 on thymic sections from one-year-old WT and *ATM*$^{-/-}$ pigs (Fig. 3B). Only cells with expected cytoplasmic immunostaining patterns (brown coloration) were considered specific to avoid possible confusion with dark staining melanocytes normally seen in the thymus of both groups. We found a reduced number of cleaved caspase 3-positive cells in the cortex of the *ATM*$^{-/-}$ thymus compared to WT, but no difference was found in the medulla (Fig. 3B).

T and B cell lymphopenia with increased CD4^{+}CD8^{+} double-positive T cells and Natural Killer (NK) cells in the peripheral blood of *ATM*$^{-/-}$ pigs

Most AT patients have immunodeficiency in both the cellular and humoral immune systems with defective B cells, lymphopenia of CD8^{+} and CD4^{+} T lymphocytes, and increased NK cells (24, 25). To determine whether *ATM*$^{-/-}$ pigs manifest similar immunological features, we performed three-colored flow cytometry to quantify CD8^{+}CD4^{+} DP T cells, NK cells,

and B cells in peripheral blood from five WT and four *ATM*$^{-/-}$ age- (2 years) and gender-matched pigs (Fig. 4). Analysis was performed after gating the lymphocytes into CD3^{-} and CD3^{+} populations. No statistically significant difference was found in the total number of lymphocytes (Supplementary Fig. 5) or in the proportion of CD4^{+} cells (WT= 23% vs. *ATM*$^{-/-}$ =31%,) (Fig. 4) between the two groups. However, the CD3^{+} cells showed a reduction in the CD8^{+} population in *ATM*$^{-/-}$ animals (WT= 35.4% vs. *ATM*$^{-/-}$ =23.8%; p<0,0001). *ATM*$^{-/-}$ pigs also had an increase in the number of CD4^{+}CD8^{+} DP cells (WT=22% vs. *ATM*$^{-/-}$ =47%, p<0.006). For the CD3^{-} lymphocyte subclass we gated the CD8^{+} and CD8^{-} populations and classified those as NK (CD3^{-}CD8^{+}) and "B-like cells" (CD3^{-}CD8^{-}) respectively, based on how they were classified previously in pigs (26, 27). These immune cell populations in *ATM*$^{-/-}$ samples were significantly increased (NK cells) or decreased (B-like cells) compared to WT [CD3^{-}CD8^{+} (NK): WT=6.6% vs. *ATM*$^{-/-}$=18%, p <0.05; CD3^{-}CD8^{-} (B-like): WT=88% vs. *ATM*$^{-/-}$ =75%; p <0.040] (Fig. 4).

Reduced IgG response to PRRS infection in *ATM*$^{-/-}$ pigs

During characterization of this porcine AT model, several pigs naturally acquired the Porcine Reproductive and Respiratory Syndrome (PRRS) virus. Positive-stranded RNA PRRS virus is a highly contagious pathogen commonly acquired by domestic pigs in North America, causing late term abortion and respiratory complications (28, 29). The pigs were tested for this virus by a standard screening method based on detection of viral nucleic acid by qPCR in the blood. IgG levels were measured in the blood of five infected WT and *ATM*$^{-/-}$ pigs (positive by qPCR). Uninfected WT and *ATM*$^{-/-}$ pigs served as negative controls for this part of the study. Viral infection caused a dramatic increase in IgG levels of WT pigs, however, the IgG response was significantly reduced in *ATM*$^{-/-}$ animals (Fig 5). Following infection, the same WT and *ATM*$^{-/-}$ pigs were vaccinated as a standard procedure to eliminate shedding of the virus. A booster vaccination was given one month after the first dose. Twenty days after each vaccination, IgG levels were retested. At both post-vaccination time points, IgG levels in *ATM*$^{-/-}$ animals were markedly lower than in the WT group (1st vaccination time point: WT=1.6 vs. *ATM*$^{-/-}$=0.4, p<0.0001; 2nd vaccination time point: WT=1.68 vs. *ATM*$^{-/-}$=0.7, p<0.001). One of the infected *ATM*$^{-/-}$ pig, which presented the lowest level of IgG at the PRRS infection time point (Fig 5), was euthanized because of the sickness and necropsy was immediately performed (Fig 2B).

DISCUSSION

Several AT mouse models have contributed to uncovering some of the intricate pathophysiological aspects of AT. Tumor formation and immunological abnormalities have been well recapitulated in these models. However, the cerebellar phenotype and the thymic lesions seen in human patients have not been clearly demonstrated, most likely because development of thymic lymphoma causes premature death within 4–5 months in these mouse models (14). Previously, we engineered a porcine *ATM*$^{-/-}$ model to bridge the gap between mouse models and AT patients. The *ATM*$^{-/-}$ pig successfully recapitulated cerebellar defects with early Purkinje cell loss, suggesting a developmental origin of the disease (18).

In the current study, we focused on pathophysiological changes outside the central nervous system (CNS), to determine if our model recapitulates other distinctive clinical manifestations of AT.

Necropsies of all organs from *ATM*$^{-/-}$ and WT pigs showed a striking anatomical defect of the female reproductive system and thymus specifically at one year of age. The uterus and ovaries of one-year-old *ATM*$^{-/-}$ pigs were similar in appearance to a young, prepubertal pig. H&E staining of *ATM*$^{-/-}$ ovaries revealed a lack of developing follicular structures that would be seen in a cycling ovary. However, the *ATM*$^{-/-}$ ovaries did exhibit some large cells reminiscent of primordial follicles, which suggests an early arrest in follicular development. While the *ATM*$^{-/-}$ uterus was small the overall structure was preserved. In humans, autopsies from AT patients have shown similar scenarios, with uteri and ovaries of infantile proportions (19, 20, 30). At the cellular level, Lin and Kim have shown a direct correlation between the *ATM* gene and meiotic maturation of porcine oocytes *in vitro*, corroborating our findings (31). Consistent with our findings, AT female pigs were infertile and had undetectable levels of circulating estrogen, a hormone produced by ovaries. To determine if infertility was a problem in male *ATM*$^{-/-}$ pigs, we analyzed their spermatozoa and ability to produce progeny when mated with WT females. Unfortunately, the number of males used in this part of the study was not enough for statistical analysis because usually males are castrated at birth; however, observed trends can still be informative. While the number and motility of spermatozoa from *ATM*$^{-/-}$ and WT pigs were similar, 50% of the spermatozoa from the mutant pigs exhibited both proximal and distal cytoplasmic droplets. Cytoplasmic droplets were described in 1909 as a cytoplasm remnant from the spermatid stage which remains attached to the spermatozoa after the maturation process (32). While their function is still unclear, the presence of cytoplasmic droplets has been associated with impaired fertility, characterized by reduced pregnancy rate and litter size in domestic species and in mice (33, 34). Mating male *ATM*$^{-/-}$ pigs with WT female pigs also resulted in a reduced conception rate and smaller litter sizes. Furthermore, there are also many reports indicating that the presence of cytoplasmic droplets in humans is similarly associated with poor spermatozoa function (35, 36). Although AT female patients with infantile gonads have been described frequently, reports of adolescent sexual features of male patients are scarce. Strich *et al.* reported a case of a 15-year-old boy with delayed puberty and testicular abnormalities (21); another report described incomplete spermatogenesis in AT male patients with generally less severe sexual features than in female AT patients (37). Two other prepuberal AT males were reported previously but these patients exhibited normal genitalia (20). However, mouse models of AT have clearly shown fertility problems owing to the absence of mature gonads and spermatozoa (14). We believe the presence of cytoplasmic droplets in spermatozoa is a manifestation of fertility impairment in *ATM*$^{-/-}$ male pigs, possibly caused by spermatogenesis defects; however, this needs to be better documented with more animals. Because of the complex regulation of gonad development and sex hormone production by the brain (hypothalamic hormones) we cannot fully exclude that hypothalamic abnormalities contribute to the reproductive failures. In fact, presence of infertility in female and partial fertility in male *ATM*$^{-/-}$ pigs would suggest the idea of a dysfunctional hypothalamo-pituitary gonadal axis (38, 39).

The direct correlation between gonad abnormalities and infertility has never been clearly proven in AT patients. However, the sterility phenotype corroborated by the absence of estradiol in the blood of *ATM*$^{-/-}$ female pigs confirms what has been previously shown in mice (14). With our *ATM*$^{-/-}$ pig model we can begin research focusing on how ATM regulates sexual development. Our *ATM*$^{-/-}$ pig can be used to investigate hormonal therapies for AT as well as for other pathologies involving sterility.

Another organ affected in AT patients is the thymus, a primary lymphoid organ where precursor immune cells arising from the bone marrow are educated and selected to become mature cells that carry out immune functions (40). In post-portem AT patients, absent or small fatty thymus lacking Hassal's corpuscle and with abnormal cortex has been shown (7, 19, 22). Conserved among species, each lobule of the thymus comprises a cortex and medulla. The thymus is a unique organ which undergoes involution with age; this involves regression in size, structure, and eventual infiltration and replacement of the organ with adipose tissue (41). Hassall's corpuscles are found in the medulla and act in both the removal of apoptotic thymocytes and the maturation of developing thymocytes.

The *ATM*$^{-/-}$ thymus at one year of age had an abnormal architecture with less medulla area, a reduced medulla:cortex ratio and fewer Hassall's corpuscles. Further support of defective thymic loss was provided by the 2.5-year-old *ATM*$^{-/-}$ pig that was euthanized due to natural PRRS virus infection. We speculate that the morbidity of this adult *ATM*$^{-/-}$ pig was caused by the establishment of a secondary infection due to compromised immunity related to the lack of ATM rather than a direct effect of the PRRS. Histological examination of the thymus of this 2.5-year-old *ATM*$^{-/-}$ pig confirmed some remaining segments of medulla and the cortex; however, Hassall's corpuscles were not observed and pronounced adipose infiltration was present. Although these observations are from only one pig, the findings support those seen in one-year-old *ATM*$^{-/-}$ pigs and importantly, reflect what has been shown in humans post-mortem. Taken together, the complete degeneration of the thymus by 2.5 years, the significant deficits in thymic structure at one year of age, and the absence of any significant differences at one month of age indicate a progressive thymic degeneration with an accelerated tendency for thymic involution during AT pathology.

The number of cleaved caspase 3-positive cells was decreased in the thymus of 1-year-old *ATM*$^{-/-}$ pigs, suggesting reduced apoptosis. Based on our observation of smaller thymi in *ATM*$^{-/-}$ pigs, this reduction in apoptosis was surprising. To further examine this matter, we also looked at cell cycle markers, such as Cdk2 and its negative regulator, p21. In *ATM*$^{-/-}$ thymi, Cdk2 expression was decreased as expected. Surprisingly, p21 levels were also decreased. To better elucidate the molecular mechanism upstream of apoptosis and the cell cycle we evaluated the level of p53 which is the central regulator of apoptosis and cell cycle and is phosphorylated by ATM and ATR (Ataxia telangiectasia and Rad3 related) (42–44). As a normal response to DNA damage, the ATM protein undergoes autophosphorylation (45, 46), and activates downstream pathways like p53, which induces cell cycle arrest to allow effective DNA repair. During lymphocyte maturation, physiological DNA "damage" is required for VDJ recombination and both p53 and ATM have been found at these recombination loci undergoing rearrangement (47). We assessed p53 total protein level and p53 phosphorylation at Ser20 and Ser15. Total p53 level were increased in *ATM*$^{-/-}$ thymi

probably due to the presence of un-repaired double-stranded DNA breaks. A higher molecular weight p53 band on Western blot proportionally decreased in the same *ATM*$^{-/-}$ samples, suggesting a reduction of phosphorylated forms of p53 as expected by the lack of ATM. However, phospho-p53(Ser15) and phospho-p53(Ser20) were undetectable in the WT or *ATM*$^{-/-}$ thymus compared to irradiated pig fibroblasts which served as the positive control. Because ATM mediates phosphorylation at several p53 sites (44, 48), we speculate that there are other p53 sites phosphorylated by ATM in the pig thymus besides Ser15 and Ser20. The lack of phosphorylation may prevent p53 from efficiently activating apoptotic mechanisms (49), as observed in *ATM*$^{-/-}$ versus WT thymus. Furthermore, the decreased expression of p21 in the *ATM*$^{-/-}$ thymus could also be due to the lack of p53 phosphorylation. However, reduced levels of the cell cycle marker Cdk2 can be explained by p53-p21 independent mechanisms (50), and reduction of this marker can also explain the shrinkage of the *ATM*$^{-/-}$ thymus.

To confirm that the thymic abnormalities seen in *ATM*$^{-/-}$ pigs affected circulating T cells as in human AT patients, we performed FACS analysis. Our results showed that the number of CD8^{+} cells and B-like cells was decreased in the blood of *ATM*$^{-/-}$ pigs compared to WT. On the other hand, we found that NK-like and CD4^{+}CD8^{+} DP cells were increased in *ATM*$^{-/-}$ pigs. In AT patients and mouse models, the numbers of CD8^{+} T cells, CD4^{+} T cells and B cells are decreased while the number of NK cells are increased (51–53). However, in our model, no difference in the percentage of CD4^{+} T cells was found. It is possible that the decrease in the number of CD8^{+} and CD4^{+} T cells in pig does not happen concomitantly and we would see the decrease of both cell populations at a later disease stage. It is possible that the *ATM*$^{-/-}$ pigs are at the beginning of this phenomena, and only the difference in the number of CD8^{+} T cells between *ATM*$^{-/-}$ and WT pigs can be discerned at this point. In the long term, it will be very informative to see if the number of CD4^{+} T cells also decreases with age. Conversely, it is possible that the unchanged CD4^{+} T cell number is a unique characteristic of the porcine immune system compared to humans. For instance, in human peripheral blood, only a small percentage of CD4^{+}CD8^{+} DP (<3%) cells are present compared to the porcine model which has 25–50% of circulating T lymphocytes as DP cells (54–56). Thus, it is difficult to compare this particular T lymphocyte population between pig and humans. In the human thymus, during the maturation of CD4^{+} and CD8^{+} single positive cells the initially CD4^{+}CD8^{+} DP cells get educated to become single-positive CD4^{+} or CD8^{+} cells The remaining DP cells that did not successfully received the commitment to become single CD4^{+} or CD8^{+} undergo caspase 3-mediated apoptosis in the cortex and only a small population (<3%) leave the thymus for the systemic circulation as CD4^{+}CD8^{+} DPcells (57). Our results show a decreased level of activated caspase 3 in the *ATM*$^{-/-}$ thymus. This could suggest that the increase of CD4+CD8+ DP cells in peripheral blood is a result of decreased apoptosis of these cells in the thymus. Yet, it is also possible that the accumulation of CD4^{+}CD8^{+} DP cells causes a problem in the maturation of CD8^{+} cells, resulting in the reduced number of CD8^{+} cells.

In addition to defects in T cell-mediated immunity, AT patients exhibit impaired response to infections and abnormal homograft rejection due to deficiency in producing select classes of immunoglobulins (58). Therefore, we examined a group of *ATM*$^{-/-}$ and WT pigs that became infected with PRRS virus. IgG levels in the sera of *ATM*$^{-/-}$ animals were

persistently lower compared to WT animals after infection and vaccination. This result is profound because it demonstrates the inability of *ATM*$^{-/-}$ pigs to produce the right amount of IgG, ultimately causing morbidity and mortality in these animals. The lower IgG level was also expected based on the low amount of B cells found in the blood of *ATM*$^{-/-}$ animals. Coincidently, the 2.5-year-old *ATM*$^{-/-}$ pig that was euthanized due to extreme sickness during the study had the lowest level of IgG. Although this was an isolated case, it suggests a correlation between low IgG levels and AT morbidity and pathology. Overall, the ability to probe both the neurological and immunological components of the disease in the AT pig model, will aid in the development of treatment protocols to ameliorate and halt the disease.

Finally, although we found functional and anatomical similarities between our porcine model and AT patients, we have not yet observed the presence of tumors in three-year-old *ATM*$^{-/-}$ pigs. AT patients have approximately 25% increased lifetime risk of developing tumors; in patients under the age of 20, leukemia and lymphoma are the most common (8). A longer study will be necessary to follow up whether tumors form in *ATM*$^{-/-}$ pigs and if so, when they begin to develop.

MATERIALS AND METHODS

Yucatan pig welfare

This study was carried out in accordance with the recommendation of the NRC *Guide for the Care of Laboratory Animals*. All animals were generated and housed in the AAALAC-accredited facilities of Exemplar Genetics. Standard procedures for animal husbandry were used throughout. The pigs were housed in groups with littermates and under the same conditions (feed, water, temperature, light etc.).

Necropsies, organ and blood collection

Organs were harvested from 1-month, 1- year and 2.5-year-old euthanized pigs (WT and *ATM*$^{-/-}$). From each pig, the following tissues were collected: cerebellum, cerebrum, eyes, thymus, gonads, lymph nodes (cervical and ileocecal), lung, stomach, kidneys, adrenals, duodenum, jejunum, ileum, spiral colon, descending colon, nasal turbinate, skin, bone marrow, uterus, vagina, urinary bladder, heart, pancreas, liver/gallbladder, thyroid, and tonsil. A board-certified veterinary pathologist (DKM) performed prosecution and examination of tissues. Each tissue was examined for gross lesions and then half of each tissue was placed in 10% neutral buffered formalin for 5–10 days at RT and processed for immunohistochemistry. The other half of each tissue was stored at −80°C until processing for Western blotting. For PRRS and estrogen detection, blood was collected by venipuncture of the jugular vein with a multi-use 20-gauge needle and 9.0 mL serum separator tube (302015 Corvac). Blood samples were centrifuged for 1,500 *g* for 10 minutes. The serum was decanted into polystyrene tubes and shipped to testing facilities for the PRRS and estrogen detection. For FACS analysis, blood was collected in EDTA 10 mL tubes (Medtonic cat number 8881311743). For semen analysis, 50 to 100 mL of semen were collected from sexually mature WT (3) and *ATM*$^{-/-}$ (2) pigs who had not been in contact with any females for one week. After ejaculation in a pre-warmed collection vessel, the

semen was kept in a cooler to reach an optimal temperature of 16 −18 °C to guarantee the best viability. The semen was shipped for analysis to Kuster Research and Consulting Inc. in Illinois.

Western blotting

Porcine thymi were lysed in ice-cold RIPA buffer and used for immunoblotting as previously described (59). In brief, a total of 60 μg of protein was subjected to NuPAGE gradient 4–15% gel electrophoresis. Separated proteins were then transferred onto nitrocellulose membranes for 2 hours at 90 V at 4°C. Blots were probed with antibodies against p53 (1:1000, Millipore), p53Ser15 (1:1000, Cell Signaling), p53Ser20 (1:1000, Cell Signaling), Cdk2 (1:1000, Cell Signaling) p21 (1:1000, Cell Signaling), caspase 3 and cleaved caspase 3 (1:1000, Cell Signaling). Anti-β-actin (1:1000, Sigma,) was used to detect β-actin as a loading control.

Histopathology and morphometric analysis

Ovary, uterus, and thymus obtained from necropsies of WT and *ATM*$^{-/-}$ female pigs at 1 month and 1 year of age were compared. For the reproductive tract, the ovaries were separated from the uterus and preserved in 10% neutral buffered formalin. The thymi were harvested and separated into two halves, one processed for histopathological analysis and the other half preserved at −80°C for molecular characterization. For histopathological examination, the tissue was processed, embedded, sectioned (~ 4μm), and stained with an antibody against cleaved caspase 3 (1:200, Cell Signaling). Morphometric analysis of the thymus structure was performed using high resolution digital images and specialized software (BX51 microscope, DP73 digital camera and CellSens software, Olympus Corp. Waltham, MA USA). Sections of thymus were evaluated for total area, medulla area, and the number of Hassall's corpuscles. From these measurements, additional data were calculated such as cortical area, cortical to medulla ratio, and number of Hassall's Corpuscles per area (total thymic or medulla). Additionally, adipose tissue infiltration, consistent with thymic involution, was quantified by evaluating the perimeter length of thymic lobules and determining percentage of adipose tissue immediately adjacent to or infiltrating into the cortex. For quantification of cells positive for cleaved caspase 3, images were taken using 20× and 60× objectives (Nikon P021) and counts were completed using Nikon NIS software. For each animal, we counted the number of cleaved caspase 3-positive cells in twelve (four inner, four middle, and four outer regions) 200 × 200 μm^2 squares of six random thymic cortex areas. Six random medulla areas were also evaluated and the positive cells within six random regions of 200 × 200 μm^2 area squares were counted. Six different cortex regions and medulla were analyzed for each animal. Each data point represents the average of these six measurements and unpaired t-test was used for the statistical analysis. For the quantification and statistical analysis, the total number of cells in cortex and medulla across six different cortical and six medullar regions were averaged for each animal.

FACS

Blood samples for phenotyping analysis were obtained from five WT and four *ATM*$^{-/-}$ female pigs at 2 years of age. The staining was performed on fresh total blood. Briefly, 50 μL of blood from each pig was mixed with 10 μL of Human Fc Receptor Binding Inhibitor

(14–9161, Ebioscience) for 30 minutes and live and dead marker (L23105, Molecular Probes) was applied for 15 minutes in the dark. The specific antibodies were added for 30 minutes in the dark at RT, erythrocytes were lysed in FACS Lyse (BD, 349202), and labeled cells were resuspended in 200 μL of FACS Buffer with 2% FBS and 0.1% sodium azide. Flow cytometry was carried out using a BD LSRFortessa cell analyzer and FlowJo v10.1 software. The three colored antibodies used were: Alexa Fluor 647-labeled mouse anti-pig CD8a (561475, BD Pharmingen), PerCP-Cy 5.5-conjugated mouse anti-pig CD3ε (BD Pharmingen 561478), and FITC-labeled mouse anti-pig CD4a (559585, BD Pharmingen). Two antibodies, Alexa Fluor 647-labeled mouse IgG2a (ab176104, Abcam) and R-phycoerythrin-labeled mouse IgG2b (559529, BD Pharmingen) were used as isogenic controls.

IgG and (E2) quantification

For IgG quantification, sera were collected from five WT and five *ATM*$^{-/-}$ infected pigs and from three WT and *ATM*$^{-/-}$ uninfected pigs as a negative control. Sera were sent to the Iowa State University Veterinary Diagnostic Laboratory where testing for PRRS antibody was performed using a commercially-available antibody test kit (IDEXX PRRS X3, 06-40959-04). Briefly, 100 μL of serum was placed into an antigen-coated plate in triplicate in parallel with negative and positive controls, and incubated for 30 minutes (±2 min) at 18–26°C. The plates were washed and an anti-porcine IgG-horseradish peroxidase conjugate was added that binds to any porcine antibody attached in the wells. Unbound conjugate was washed away and 3,3′,5,5 tetramethylbenzidine (TMB) substrate was added to the wells. After stopping the reaction, the optical density (OD) was measured at 650 nm. Color development is proportional to the amount of specific antibodies against PRRSV present in the sample. The sample/positive control value (S/P) was calculated for each sample from the ODs of the sample, the positive control sera, and the negative control sera. The interpretation of the S/P value is based on whether it is below the positive/negative S/P cutoff value (0.400). S/P values greater than or equal to 0.400 are interpreted as positive. The IgG level was measured as absorbance ratio between sample OD/positive sample OD. One-way ANOVA was used to measure the statistical significance of IgG induction between non-infected and infected groups and the two-way ANOVA was used for the following measurements at the three different time points between WT and *ATM*$^{-/-}$ groups. For the Estradiol measurements, three WT and *ATM*$^{-/-}$ sexually mature females were synchronized for estrus by administration of 6.8 mL (15 mg Altrenogest-Matrix ® (Merck 003488) per female for 14 days. Blood was collected 4 days after the last dose and sent to UnityPoint Health for E2 measurements. Measurement of Estradiol was performed by an **e**lectro**c**hemi**l**uminescence **i**mmuno**a**ssay “ECLIA”(Roche Diagnostics).

STATISTICAL ANALYSIS

Statistical analysis was performed using GraphPad Prism software version 6.0 (GraphPad La Jolla CA, USA). Cleaved caspase 3 staining analysis and comparison of T and B cell flow cytometric data were analyzed by two-tailed unpaired t-tests. Differences were considered statistically significant when $p \leq 0.05$. For the IgG immunological response to PRRS infection one- and two-way ANOVAs were used.

Supplementary Material

Refer to Web version on PubMed Central for supplementary material.

Acknowledgments

Assistance was provided by the Sanford Research Molecular Pathology and Imaging Core and by the University of Iowa Carver College of Medicine, Comparative Pathology Laboratory for assistance with histological analysis. We thank Logan Langin for help with the pig behavior study and Marisela Killian for assistance in the cytofluorometry core at Sanford Research.

FUNDING

This work was supported by Sanford Research and the National Institute of Health COBRE Projects (grant number P20 GM103620, P20 GM103548 and by a National Institute of Health SBIR grant to Exemplar Genetics (grant number R44NS076075).

References

1. Swift M, Morrell D, Cromartie E, Chamberlin AR, Skolnick MH, Bishop DT. The incidence and gene frequency of ataxia-telangiectasia in the United States. American journal of human genetics. 1986; 39(5):573–83. [PubMed: 3788973]
2. Boder E. Ataxia-telangiectasia: some historic, clinical and pathologic observations. Birth defects original article series. 1975; 11(1):255–70.
3. Sedgewick RPaBE. Ataxia-telangiectasia. Handbook of Clinical Neurology. 1991:347–423.
4. Taylor AM, Metcalfe JA, Thick J, Mak YF. Leukemia and lymphoma in ataxia telangiectasia. Blood. 1996; 87(2):423–38. [PubMed: 8555463]
5. Makis A, Polychronopoulou S, Haidas S. Osteosarcoma as a second tumor after treatment for primary non-Hodgkin's lymphoma in a child with ataxia-telangiectasia: presentation of a case and review of possible pathogenetic mechanisms. Journal of pediatric hematology/oncology. 2004; 26(7):444–6. [PubMed: 15218420]
6. Suarez F, Mahlaoui N, Canioni D, Andriamanga C, Dubois d'Enghien C, Brousse N, et al. Incidence, presentation, and prognosis of malignancies in ataxia-telangiectasia: a report from the French national registry of primary immune deficiencies. Journal of clinical oncology : official journal of the American Society of Clinical Oncology. 2015; 33(2):202–8. [PubMed: 25488969]
7. Strich, Sj. Pathological findings in three cases of ataxia-telangiectasia. 1966:29.
8. Rothblum-Oviatt C, Wright J, Lefton-Greif MA, McGrath-Morrow SA, Crawford TO, Lederman HM. Ataxia telangiectasia: a review. Orphanet journal of rare diseases. 2016; 11(1):159. [PubMed: 27884168]
9. McGrath-Morrow SA, Gower WA, Rothblum-Oviatt C, Brody AS, Langston C, Fan LL, et al. Evaluation and management of pulmonary disease in ataxia-telangiectasia. Pediatric pulmonology. 2010; 45(9):847–59. [PubMed: 20583220]
10. Shiloh Y, Ziv Y. The ATM protein kinase: regulating the cellular response to genotoxic stress, and more. Nature reviews Molecular cell biology. 2013; 14(4):197–210.
11. Gatti RA, Berkel I, Boder E, Braedt G, Charmley P, Concannon P, et al. Localization of an ataxia-telangiectasia gene to chromosome 11q22–23. Nature. 1988; 336(6199):577–80. [PubMed: 3200306]
12. Verhagen MM, Last JI, Hogervorst FB, Smeets DF, Roeleveld N, Verheijen F, et al. Presence of ATM protein and residual kinase activity correlates with the phenotype in ataxia-telangiectasia: a genotype-phenotype study. Human mutation. 2012; 33(3):561–71. [PubMed: 22213089]
13. Taylor AM, Lam Z, Last JI, Byrd PJ. Ataxia telangiectasia: more variation at clinical and cellular levels. Clinical genetics. 2015; 87(3):199–208. [PubMed: 25040471]
14. Barlow C, Hirotsune S, Paylor R, Liyanage M, Eckhaus M, Collins F, et al. Atm-deficient mice: a paradigm of ataxia telangiectasia. Cell. 1996; 86(1):159–71. [PubMed: 8689683]

15. Imamura S, Kishi S. Molecular cloning and functional characterization of zebrafish ATM. The international journal of biochemistry & cell biology. 2005; 37(5):1105–16. [PubMed: 15743681]
16. Petersen AJ, Katzenberger RJ, Wassarman DA. The innate immune response transcription factor relish is necessary for neurodegeneration in a Drosophila model of ataxia-telangiectasia. Genetics. 2013; 194(1):133–42. [PubMed: 23502677]
17. Quek H, Luff J, Cheung K, Kozlov S, Gatei M, Lee CS, et al. A rat model of ataxia-telangiectasia: evidence for a neurodegenerative phenotype. Human molecular genetics. 2017; 26(1):109–23. [PubMed: 28007901]
18. Beraldi R, Chan CH, Rogers CS, Kovacs AD, Meyerholz DK, Trantzas C, et al. A novel porcine model of ataxia telangiectasia reproduces neurological features and motor deficits of human disease. Human molecular genetics. 2015; 24(22):6473–84. [PubMed: 26374845]
19. Miller ME, Chatten J. Ovarian changes in ataxia telangiectasia. Acta paediatrica Scandinavica. 1967; 56(5):559–61. [PubMed: 6050359]
20. Zadik Z, Levin S, Prager-Lewin R, Laron Z. Gonadal dysfunction in patients with ataxia telangiectasia. Acta paediatrica Scandinavica. 1978; 67(4):477–9. [PubMed: 354315]
21. S SJ. Pathological findings in three cases of ataxia-telangiectasia. J neurol NeurosurgPsychiat. 1966; 29:489–99.
22. Peterson RD, Kelly WD, Good RA. Ataxia-Telangiectasia. Its Association with a Defective Thymus, Immunological-Deficiency Disease, and Malignancy. Lancet. 1964; 1(7344):1189–93. [PubMed: 14132657]
23. Peterson RD, Cooper MD, Good RA. Lymphoid tissue abnormalities associated with ataxia-telangiectasia. The American journal of medicine. 1966; 41(3):342–59. [PubMed: 5914110]
24. Schubert R, Reichenbach J, Zielen S. Deficiencies in CD4+ and CD8+ T cell subsets in ataxia telangiectasia. Clinical and experimental immunology. 2002; 129(1):125–32. [PubMed: 12100032]
25. Staples ER, McDermott EM, Reiman A, Byrd PJ, Ritchie S, Taylor AM, et al. Immunodeficiency in ataxia telangiectasia is correlated strongly with the presence of two null mutations in the ataxia telangiectasia mutated gene. Clinical and experimental immunology. 2008; 153(2):214–20. [PubMed: 18505428]
26. Gerner W, Kaser T, Saalmuller A. Porcine T lymphocytes and NK cells–an update. Developmental and comparative immunology. 2009; 33(3):310–20. [PubMed: 18601948]
27. Butler JE, Lager KM, Splichal I, Francis D, Kacskovics I, Sinkora M, et al. The piglet as a model for B cell and immune system development. Veterinary immunology and immunopathology. 2009; 128(1–3):147–70. [PubMed: 19056129]
28. Collins JE, Benfield DA, Christianson WT, Harris L, Hennings JC, Shaw DP, et al. Isolation of swine infertility and respiratory syndrome virus (isolate ATCC VR-2332) in North America and experimental reproduction of the disease in gnotobiotic pigs. Journal of veterinary diagnostic investigation : official publication of the American Association of Veterinary Laboratory Diagnosticians, Inc. 1992; 4(2):117–26.
29. Rowland R, Lunney J, Dekkers J. Control of porcine reproductive and respiratory syndrome (PRRS) through genetic improvements in disease resistance and tolerance. Frontiers in Genetics. 2012; 3(260)
30. Nissenkorn A, Levy-Shraga Y, Banet-Levi Y, Lahad A, Sarouk I, Modan-Moses D. Endocrine abnormalities in ataxia telangiectasia: findings from a national cohort. Pediatric research. 2016; 79(6):889–94. [PubMed: 26891003]
31. Lin ZL, Kim NH. Role of ataxia-telangiectasia mutated (ATM) in porcine oocyte in vitro maturation. Cell biology international. 2015; 39(6):710–20. [PubMed: 25598069]
32. G R. Die Spermien der Nagetiere. Biology Untersuch NFJena. 1909; 14(133):153–6.
33. Waberski D, Meding S, Dirksen G, Weitze KF, Leiding C, Hahn R. Fertility of long-term-stored boar semen: Influence of extender (Androhep and Kiev), storage time and plasma droplets in the semen. ANIMAL REPRODUCTION SCIENCE. 1994; 36(1–2):145–51.
34. Yeung CH, Wagenfeld A, Nieschlag E, Cooper TG. The cause of infertility of male c-ros tyrosine kinase receptor knockout mice. Biology of reproduction. 2000; 63(2):612–8. [PubMed: 10906072]

35. Zini A, Defreitas G, Freeman M, Hechter S, Jarvi K. Varicocele is associated with abnormal retention of cytoplasmic droplets by human spermatozoa. Fertility and sterility. 2000; 74(3):461–4. [PubMed: 10973638]
36. Mak V, Jarvi K, Buckspan M, Freeman M, Hechter S, Zini A. Smoking is associated with the retention of cytoplasm by human spermatozoa. Urology. 2000; 56(3):463–6. [PubMed: 10962316]
37. Aguilar MJ, Kamoshita S, Landing BH, Boder E, Sedgwick RP. Pathological observations in ataxia-telangiectasia. A report of five cases. Journal of neuropathology and experimental neurology. 1968; 27(4):659–76. [PubMed: 5687758]
38. Padmanabhan V, Karsch FJ, Lee JS. Hypothalamic, pituitary and gonadal regulation of FSH. Reproduction. 2002; 59:67–82. [PubMed: 12698974]
39. Plant TM. 60 YEARS OF NEUROENDOCRINOLOGY: The hypothalamo-pituitary-gonadal axis. The Journal of endocrinology. 2015; 226(2):T41–54. [PubMed: 25901041]
40. Germain RN. T-cell development and the CD4-CD8 lineage decision. Nature reviews Immunology. 2002; 2(5):309–22.
41. Gui J, Mustachio LM, Su DM, Craig RW. Thymus Size and Age-related Thymic Involution: Early Programming, Sexual Dimorphism, Progenitors and Stroma. Aging and disease. 2012; 3(3):280–90. [PubMed: 22724086]
42. Marechal A, Zou L. DNA damage sensing by the ATM and ATR kinases. Cold Spring Harbor perspectives in biology. 2013; 5(9)
43. Tibbetts RS, Brumbaugh KM, Williams JM, Sarkaria JN, Cliby WA, Shieh SY, et al. A role for ATR in the DNA damage-induced phosphorylation of p53. Genes & development. 1999; 13(2): 152–7. [PubMed: 9925639]
44. Saito S, Goodarzi AA, Higashimoto Y, Noda Y, Lees-Miller SP, Appella E, et al. ATM mediates phosphorylation at multiple p53 sites, including Ser(46), in response to ionizing radiation. The Journal of biological chemistry. 2002; 277(15):12491–4. [PubMed: 11875057]
45. Bakkenist CJ, Kastan MB. DNA damage activates ATM through intermolecular autophosphorylation and dimer dissociation. Nature. 2003; 421(6922):499–506. [PubMed: 12556884]
46. Lee JH, Paull TT. ATM activation by DNA double-strand breaks through the Mre11-Rad50-Nbs1 complex. Science. 2005; 308(5721):551–4. [PubMed: 15790808]
47. Perkins EJ, Nair A, Cowley DO, Van Dyke T, Chang Y, Ramsden DA. Sensing of intermediates in V(D)J recombination by ATM. Genes & development. 2002; 16(2):159–64. [PubMed: 11799059]
48. Kodama M, Otsubo C, Hirota T, Yokota J, Enari M, Taya Y. Requirement of ATM for rapid p53 phosphorylation at Ser46 without Ser/Thr-Gln sequences. Molecular and cellular biology. 2010; 30(7):1620–33. [PubMed: 20123963]
49. Fridman JS, Lowe SW. Control of apoptosis by p53. Oncogene. 2003; 22(56):9030–40. [PubMed: 14663481]
50. Berns K, Martins C, Dannenberg JH, Berns A, te Riele H, Bernards R. p27kip1-independent cell cycle regulation by MYC. Oncogene. 2000; 19(42):4822–7. [PubMed: 11039898]
51. Nowak-Wegrzyn A, Crawford TO, Winkelstein JA, Carson KA, Lederman HM. Immunodeficiency and infections in ataxia-telangiectasia. The Journal of pediatrics. 2004; 144(4):505–11. [PubMed: 15069401]
52. Giovannetti A, Mazzetta F, Caprini E, Aiuti A, Marziali M, Pierdominici M, et al. Skewed T-cell receptor repertoire, decreased thymic output, and predominance of terminally differentiated T cells in ataxia telangiectasia. Blood. 2002; 100(12):4082–9. [PubMed: 12393664]
53. Carney EF, Srinivasan V, Moss PA, Taylor AM. Classical ataxia telangiectasia patients have a congenitally aged immune system with high expression of CD95. Journal of immunology. 2012; 189(1):261–8.
54. Zuckermann FA, Husmann RJ. Functional and phenotypic analysis of porcine peripheral blood CD4/CD8 double-positive T cells. Immunology. 1996; 87(3):500–12. [PubMed: 8778040]
55. Blue ML, Daley JF, Levine H, Schlossman SF. Coexpression of T4 and T8 on peripheral blood T cells demonstrated by two-color fluorescence flow cytometry. Journal of immunology. 1985; 134(4):2281–6.

56. Patel SS, Wacholtz MC, Duby AD, Thiele DL, Lipsky PE. Analysis of the functional capabilities of CD3+CD4−CD8− and CD3+CD4+CD8+ human T cell clones. Journal of immunology. 1989; 143(4):1108–17.

57. Jiang D, Zheng L, Lenardo MJ. Caspases in T-cell receptor-induced thymocyte apoptosis. Cell death and differentiation. 1999; 6(5):402–11. [PubMed: 10381640]

58. Eisen AH, Karpati G, Laszlo T, Andermann F, Robb JP, Bacal HL. Immunologic Deficiency in Ataxia Telangiectasia. The New England journal of medicine. 1965; 272:18–22. [PubMed: 14219207]

59. Beraldi R, Li X, Martinez Fernandez A, Reyes S, Secreto F, Terzic A, et al. Rbm20-deficient cardiogenesis reveals early disruption of RNA processing and sarcomere remodeling establishing a developmental etiology for dilated cardiomyopathy. Human molecular genetics. 2014; 23(14): 3779–91. [PubMed: 24584570]

Highlights

- The A-T porcine model recapitulates multi-system abnormalities similar to the human disease.”
- AT porcine model shows infertility associated with a low estradiol level in blood
- AT porcine model shows a reduced immunological response to PRRS viral infection
- Apoptosis and P53 are involved in the thymus pathology in AT pigs
- Altered cell cycle is involved in the thymus pathology of AT pigs

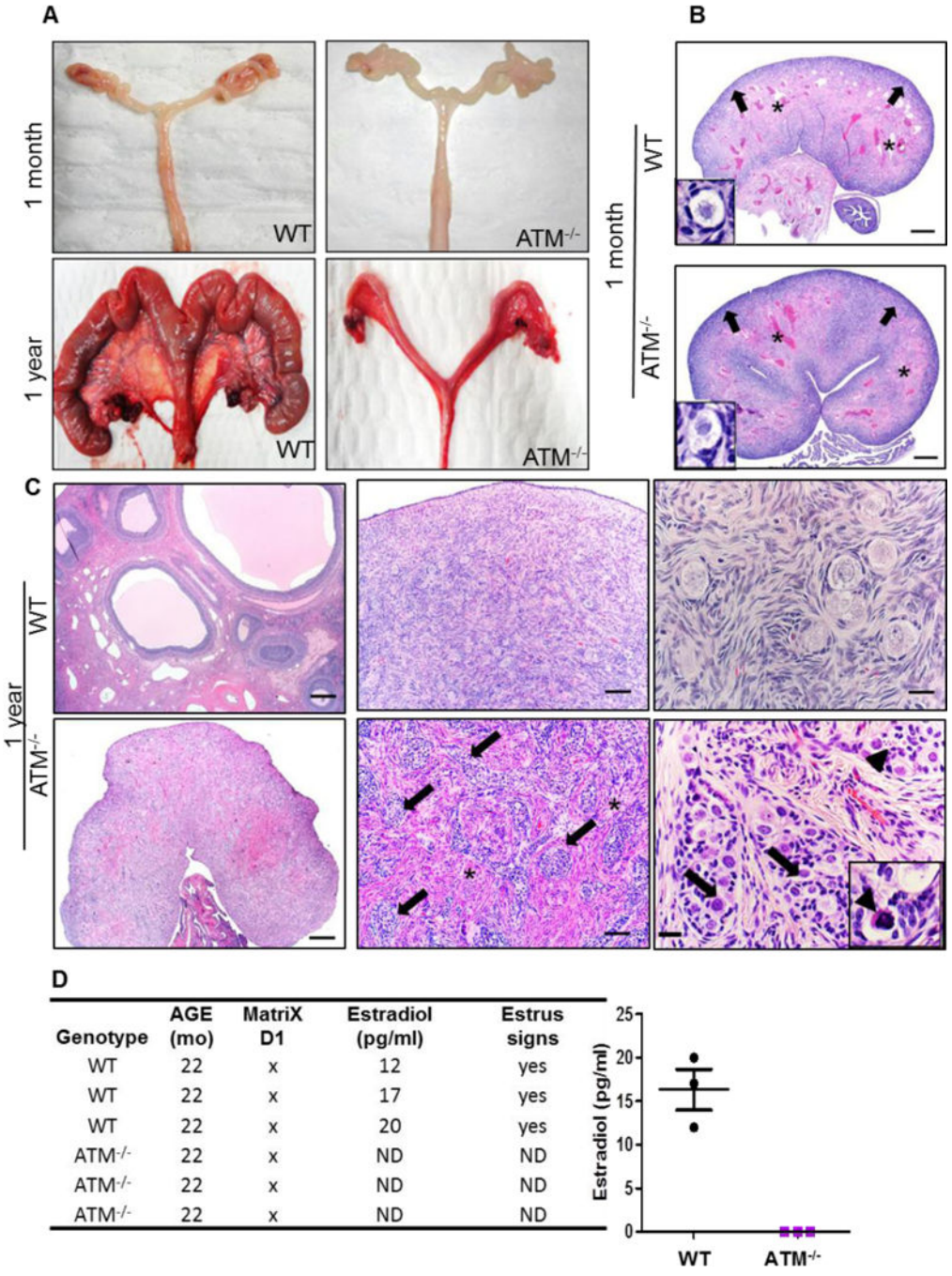

Genotype	AGE (mo)	MatriX D1	Estradiol (pg/ml)	Estrus signs
WT	22	x	12	yes
WT	22	x	17	yes
WT	22	x	20	yes
ATM-/-	22	x	ND	ND
ATM-/-	22	x	ND	ND
ATM-/-	22	x	ND	ND

Fig. 1. Structural and functional abnormalities in the reproductive system of ATM$^{-/-}$ female pigs

A) Macroscopic appearance of ovaries and uterus of WT (CTRL) and *ATM*$^{-/-}$ pigs at 1 month and 1 year of age. Images were taken at equal magnification. Compared to WT, adult (1-year-old) *ATM*$^{-/-}$ female pigs had smaller ovaries and uterus. **B**) Haematoxylin and Eosin (HE) staining showed that ovaries of both groups at 1 month of age were composed mostly of fibrovascular tissue stroma (asterisks), and primordial follicles (insets) were located principally in the cortex region (arrows). Scale bars 500μm **C**) H&E staining of WT and *ATM*$^{-/-}$ ovaries at 1 year showed the overall structure of the ovaries (left images). *ATM*$^{-/-}$

ovaries were composed of cortical cords/nests (arrows, bottom middle image) on a fibrovascular stroma (asterisks) that frequently gave rise to larger cells (arrows, bottom right image). These features along with the smaller size of the *ATM*$^{-/-}$ ovaries were reminiscent to prepubertal ovaries. *ATM*$^{-/-}$ ovaries lacked the extent of primordial follicles that were typical in the cortex of WT ovaries (arrows, top right image). Scale bars from the left to right figures: 500μm-100μm-25μm **D)** Table and graph show the quantification of estradiol (E2) in the blood of sexually mature WT and *ATM*$^{-/-}$ females. ND: none detected.

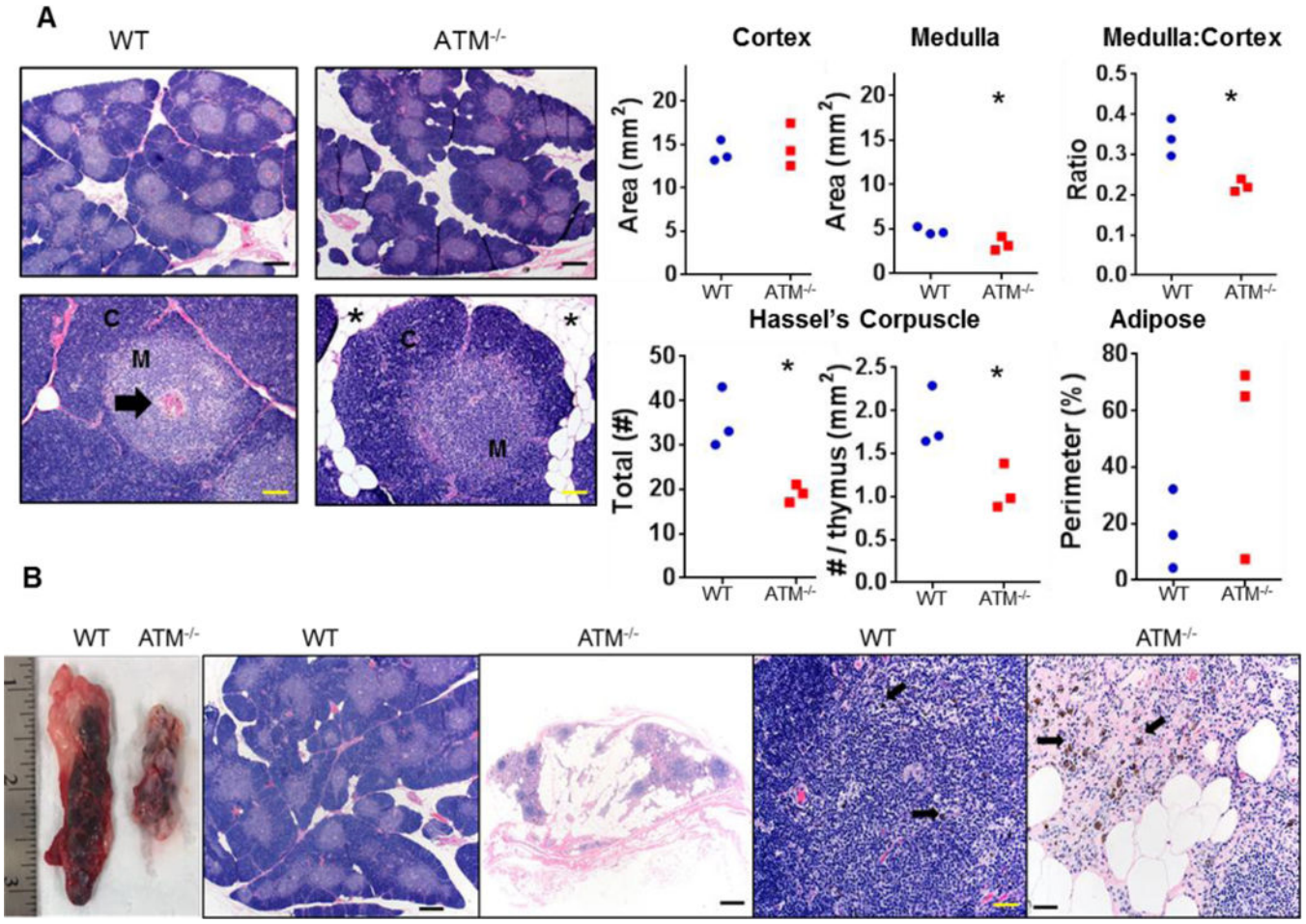

Fig. 2. Thymic abnormalities in *ATM*$^{-/-}$ pigs

A) Representative images of thymus lobules by H&E staining and morphometric analysis of thymi from 3 *ATM*$^{-/-}$ and 3 WT female pigs at 1 year of age. The thymic lobules were characterized by a cortex (C) surrounding a medulla (M) with scattered Hassall's corpuscles (arrow). The thymic cortex area was similar for WT and *ATM*$^{-/-}$ pigs; however, the medulla area and the medulla:cortex ratio were both decreased in mutant pigs ($p<0.05$). The total number of Hassall's corpuscles and the number normalized to thymus area were both reduced ($p<0.05$) in *ATM*$^{-/-}$ versus WT pigs. The extent of adipose infiltration (asterisk) trended higher in *ATM*$^{-/-}$ versus WT pigs. Scale bars top panel 500μm, bottom panel 100 μm **B)** Examination of thymi in *ATM*$^{-/-}$ and WT pigs at 2.5 years of age. H&E staining showed normal structure of the WT thymus. *ATM*$^{-/-}$ pigs lacked evidence of thymic tissue and was replaced by adipose and scattered lymphoid tissue. Note that melanocytes (arrows, pigmented cells) were commonly found and expected in the thymus tissue of WT pigs, remnant lymphoid tissues had scattered pigmented cells. Thymic morphometry was assessed by unpaired t-test with significance placed at * $p<0.05$. Scale bars: from left to right figures: 500μm-500μm-50μm-50μm

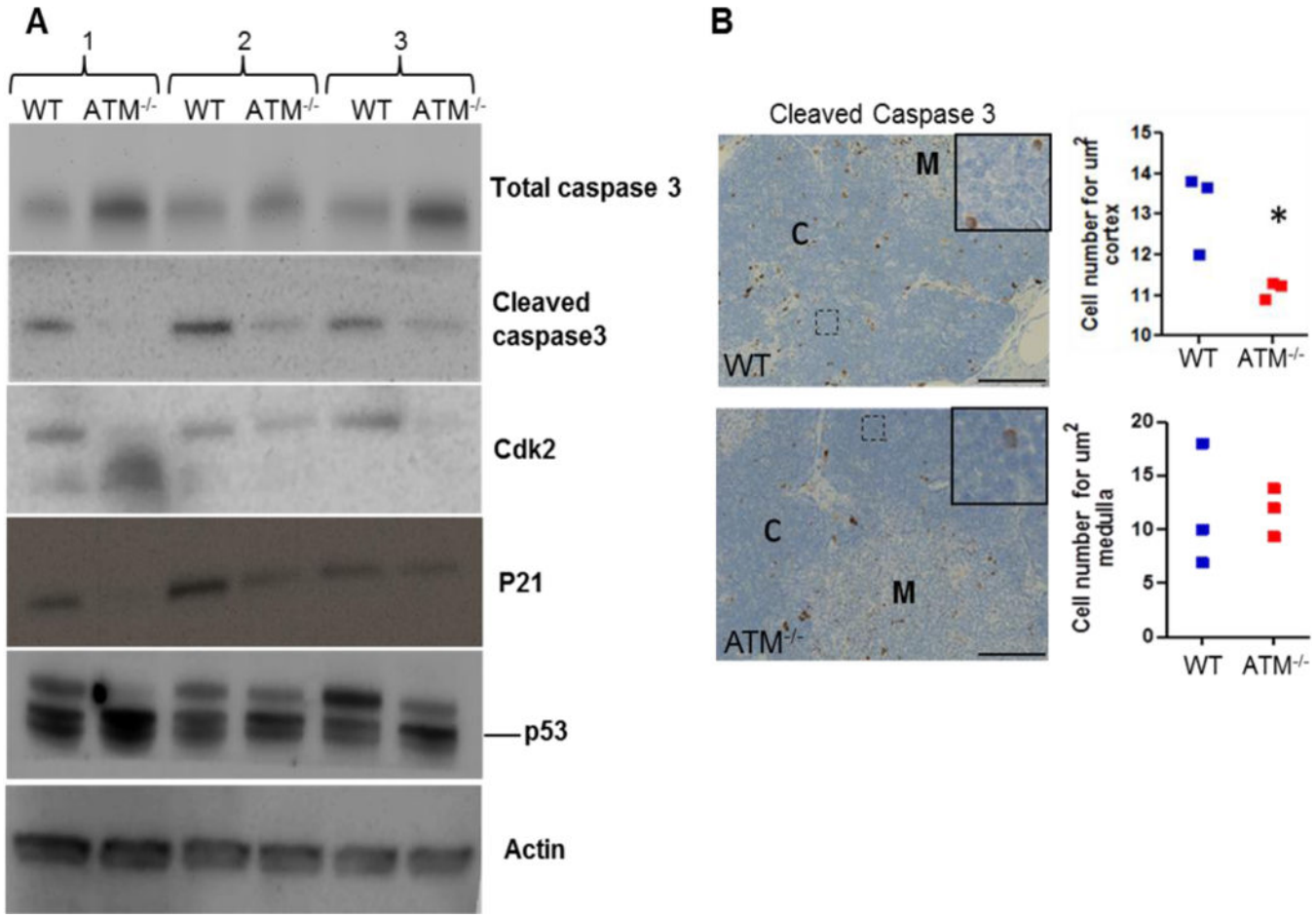

Fig. 3. Decreased apoptosis and cell cycle arrest in the *ATM*$^{-/-}$ thymus

A) Representative Western blots show decreased level of cleaved caspase 3 and accumulation of total caspase in the thymus of three different 1-year-old ATM$^{-/-}$ pigs compared to age- and gender-matched WT pigs. Cdk2 and p21 expression, markers for cell cycle progression, were also reduced in *ATM*$^{-/-}$ samples. However, total p53 level was increased in *ATM*$^{-/-}$ thymus samples. Actin was used as a loading control. **B)** Immunostaining for cleaved caspase 3 was used to quantify apoptotic cells in the cortex and medulla of the thymus (3 *ATM*$^{-/-}$ and 3 WT pigs at 1 year of age). Each data point in the graphs represents the average apoptotic cell number across 5 samples in cortex or medulla for each animal. Unpaired t-test was used for statistical analysis (*p=0.02). Scale bar, 100 μm. M: medulla and C: cortex

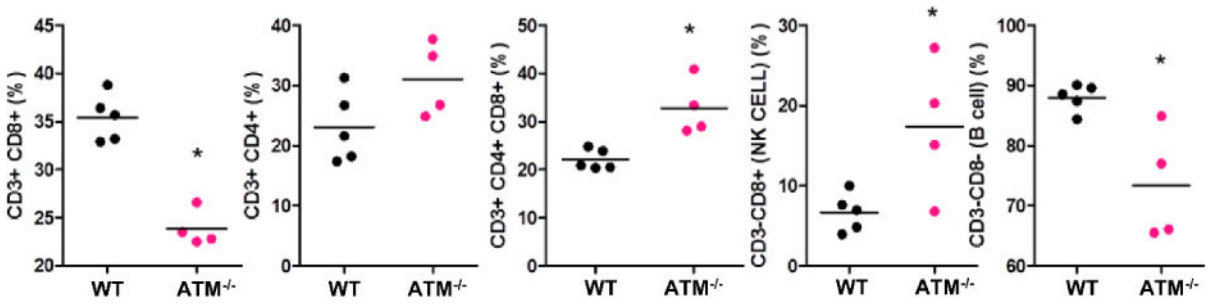

Fig. 4. T and B cell lymphopenia with increased $CD4^+CD8^+$ double-positive T and natural killer (NK) cells in the peripheral blood of *ATM*$^{-/-}$ pigs

Graphs represent the percentage of $CD8^+$, $CD4^+$, $CD4^+CD8^+$ double-positive, NK cells, and B cells in peripheral blood from five WT and four *ATM*$^{-/-}$ pigs at 2 years of age. Each data point represents the average of technical triplicates per pig sample. Analysis was performed using FlowJo V10.1 and statistical analysis between the 2 groups was performed by 2-tailed t-test with Welch's correction for the $CD3^-CD8^+$ and $CD3^-CD8^-$ cell populations (*$p<0.05$).

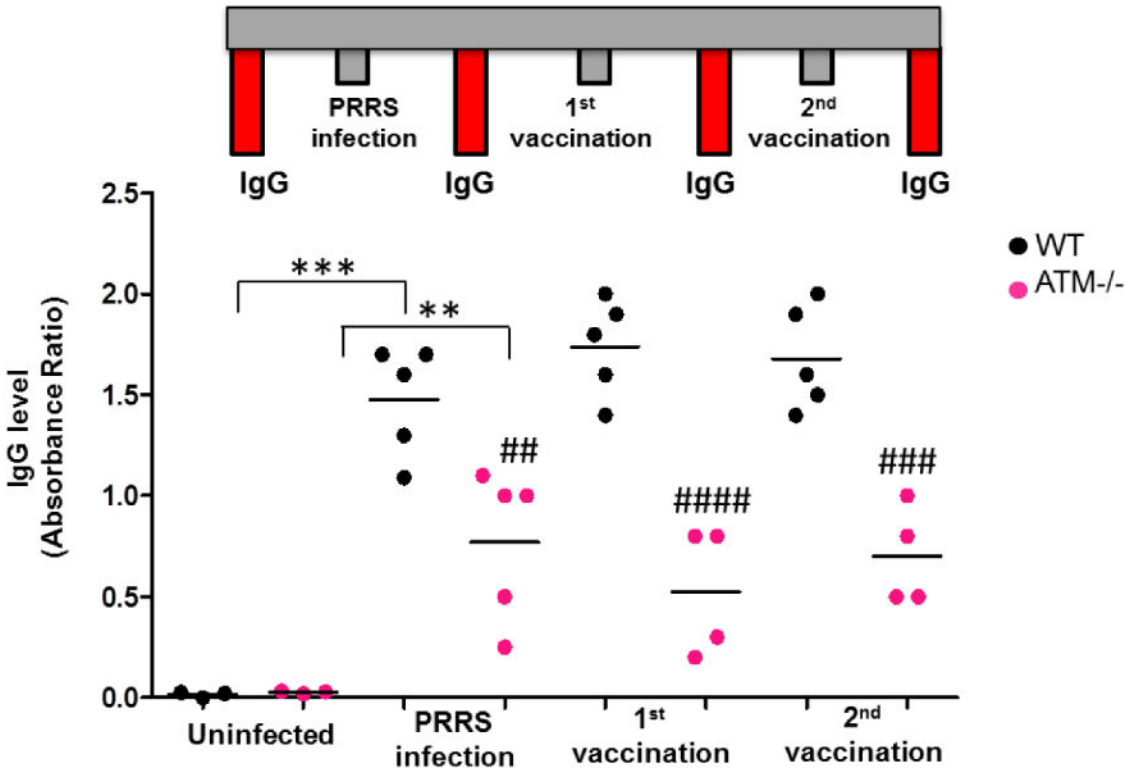

Fig. 5. Reduced IgG response to PRRS virus infection in *ATM*$^{-/-}$ pigs

The diagram depicts the steps of PRRS natural infection, vaccinations, and the four time points when IgG levels were measured in WT and *ATM*$^{-/-}$ pigs. IgG levels in serum samples were measured by ELISA at four time points: before infection, after infection, after the 1st dose of vaccination and after the 2nd dose of vaccination. IgG levels were graphed as an absorbance ratio of the sample OD/positive control OD. Each data point represents an animal, and statistical analysis was performed by one-way ANOVA for the IgG levels between the non-infected group and the infected group, showing statistically significant induction of IgG in WT and *ATM*$^{-/-}$ pigs (*** $p<0.0001$ and ** $p<0.001$). Two-way ANOVA was used to compare the WT and *ATM*$^{-/-}$ groups across the 3 time points (## $p<0.01$; #### $p<0.0001$; ### $p<0.001$).